A phase mixture model for anisotropic creep of forged Al–Cu–Mg–Si alloy

Konstantin Naumenko [a,*], Elisabetta Gariboldi [b]

[a] Otto-von-Guericke-University Magdeburg, Institute of Mechanics, D-39106 Magdeburg, Germany
[b] Politecnico di Milano, Department of Mechanical Engineering, Via La Masa 34 20156 Milano, Italy

Received 22 July 2014
Received in revised form
5 September 2014
Accepted 6 September 2014
Available online 16 September 2014

1. Introduction

Age-hardenable alloys based on the aluminum-copper system (known as AA2xxx alloys) exhibit superior creep strength and are widely used in structural components operating at elevated temperatures [1,2]. Complex shape parts produced from these alloys usually exhibit microstructural anisotropy as a result of processing [3]. Furthermore, the creep properties of age-hardenable alloys strongly depend on the heat treatment and ageing conditions [4].

For the simulation of processing as well as for structural analysis a constitutive model is required. Such a model should reflect deformation, hardening/recovery, ageing and damage mechanisms for the considered alloy under mechanical loading and thermal environment. The model must also be compatible with methods of structural mechanics to enable the finite element analysis of real components under multi-axial stress state. Unified constitutive models of inelastic deformation are available for many high-temperature materials, e.g. heat-resistant steels, nickel-based alloys and cast irons [5–7]. The basic ingredients include a constitutive equation for the inelastic strain rate tensor and evolution equations for internal state variables that capture changes in the microstructure. One feature of age-hardenable aluminum alloys is the essential influence of exposure time on the creep strength at elevated temperature. In [8] a creep constitutive equation with three scalar state variables – the hardening variable, the ageing variable and the damage variable is developed. The overageing process is explicitly described by a kinetic equation according to the Ostwald ripening theory. The material parameters in constitutive and evolution equations are identified from creep curves for the aluminum alloy BS 1742 at 150 °C. A similar model is developed and applied to the analysis of creep age forming processes in [9]. The material parameters are given for alloys AA2324 and AA7B04. Creep strength and overageing processes of aluminum alloys are affected by the shape of precipitates. Kinetic equations for the coarsening of rod-shaped or plate-shaped particles are presented and identified for AA2124 in [10].

Several approaches to describe hardening/recovery processes in aluminum alloys are discussed in the literature. In [8]

* Corresponding author.
E-mail addresses: konstantin.naumenko@ovgu.de (K. Naumenko), elisabetta.gariboldi@polimi.it (E. Gariboldi).

a phenomenological scalar-valued hardening parameter enters the constitutive equation to capture the primary creep stage. In [11] a kinematic hardening model with the backstress deviator is applied to describe creep ratcheting. In [12–14] the mean dislocation density and the characteristic particle size are used as internal state variables. The threshold stress is introduced as a sum of dislocation (Taylor-type) and precipitate (Orowan-type) contributions.

Tertiary creep is usually described by damage, overageing and/or softening variables and corresponding evolution equations. In [15,16] a single damage state variable is utilized to reflect all processes leading to the tertiary creep stage for AA2024. In [8,9] two independent state variables and kinetic equations are introduced to capture overageing and cavitation processes leading to accelerated creep.

Aluminium alloys often exhibit anisotropic creep properties as a result of processing [3]. Anisotropic response can also be induced during the creep exposure [17]. Origins of anisotropic creep include elongated grains, crystallographic texture, non-uniform distribution of particles, oriented grain boundary cavities, etc. The classical approach to formulate a constitutive equation for anisotropic creep is based on the theory of symmetries and representation of tensor-valued functions [18,17]. For the assumed symmetry class, e.g. a transverse isotropy, a creep potential is formulated as a function of appropriate invariants of the stress tensor. The resulting creep constitutive equation includes a number of material parameters to be identified from experimental creep curves for different stress states and different loading directions. This approach provides a general form of a constitutive equation. However, the identification of all required parameters is usually not feasible since the required experimental creep curves are rarely available.

The aim of this paper is to analyze creep behavior of forged AA2014 alloy and to develop an alternative approach to reflect the dependence of the creep rates on the loading direction. Basic microstructural features and creep curves for the temperature range 130–170 °C and several stress levels in two loading directions are presented. With the given experimental data origins of anisotropic creep will be explained with the help of a phase mixture (composite) model of inelastic deformation. To formulate the model, constitutive equations for individual phases and an anisotropic interaction rule will be introduced. With additional state variables including the normalized dislocation density and the normalized particle size as well as corresponding evolution equations, hardening/recovery and overageing processes will be described. Through a change of variables the model will be reduced to a set of kinetic equations such that the material parameters can be identified from families of creep curves for two loading directions. The results of identification are presented for the temperature of 150 °C and several stress levels.

2. Basic features of microstructure and creep behavior

The material investigated is an Al–4.4Cu–0.5Mg–0.9Si–0.8Mn alloy (IADS 2014 grade). An extruded bar from this alloy was axisymmetrically forged to produce a cave cylinder with the length of 230 mm and an external diameter of 190 mm. Let us designate three directions of a cylindrical forging as follows: the longitudinal (axial) by L, the tangential (circumferential) by T and the radial by R.

Two sets of $20 \times 20 \times 100$ mm^3 bars were sampled from the as supplied forging with their longer side in L and T directions, respectively. Tension tests were performed at temperatures within the range 20-170 °C. Creep tests were conducted under constant load at 130 °C, 150 °C and 170 °C (homologous temperature range 0.44 – 0.49) under stresses that led to a range of times to rupture from several hours to more than 10000 h. Crept specimens were diametrally cut in order to investigate microstructure features along the gauge length.

The investigated forgings were characterized by grains elongated in the main plastic flow path experienced during the processing. Their mean size of grains was about 300, 80, 50 μm along the L, T and R directions, respectively. Fig. 1 shows light optical microscope micrographs of the microstructure of the forged part in 2014 alloy in different metallographic sections.

Two kinds of coarse intermetallic particles were present in the microstructure: globular Al_2Cu (θ) particles (bright particles in Fig. 1) and blocky shaped clustered particles containing Fe, Mn, Si and Cu (darker particles in Fig. 1). These latter secondary phase clustered particles are elongated in the L direction. In most of the volume of the forging, macrographic analyzes revealed the large intermetallic particles longitudinally oriented, suggesting the same direction of the plastic flow during the processing.

In addition, transmission electron microscopy images published in [19] illustrate the presence of θ' phase, in the form of rod-like precipitates aligned along the ⟨001⟩ crystallographic directions of the α-Al matrix. These precipitates play an important role in strengthening of the alloy. It was supplied in the T6 condition, that is the solution treatment at 778 K and aging at 433 K for 16 h. During the subsequent creep overageing processes take place leading to the increase of particles size and distance between particles with time.

Creep curves for three mentioned temperature levels and for stresses in the range 200–400 MPa were smoothed to compute

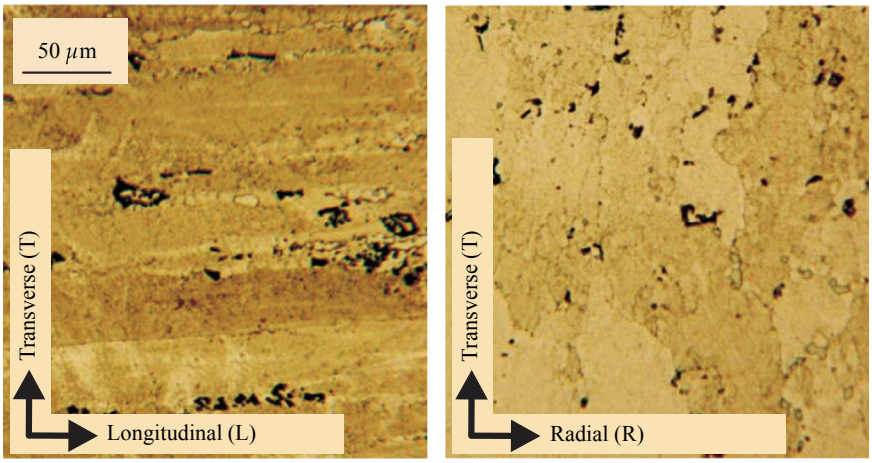

Fig. 1. Light optical microscope micrographs of the forged part from AA2014 in different metallographic sections.

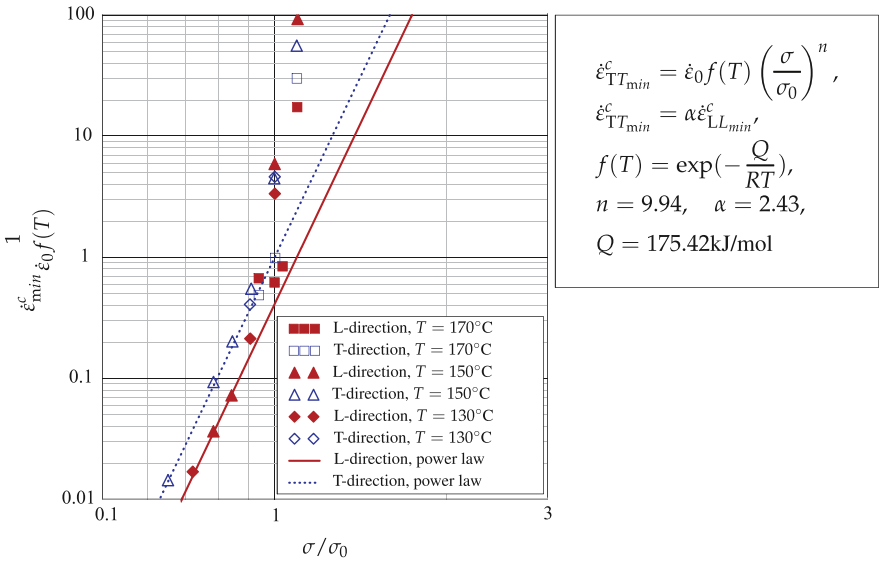

Fig. 2. Normalized minimum creep rate vs. normalized stress for longitudinal and transverse creep tests of AA2014 at different temperature levels.

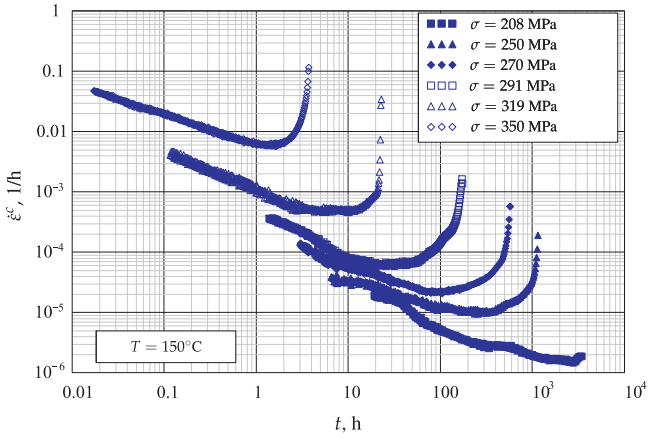

Fig. 3. Creep rate vs. time curves in transverse direction of AA2014 for $T = 150^{\circ}$ C and different stress levels.

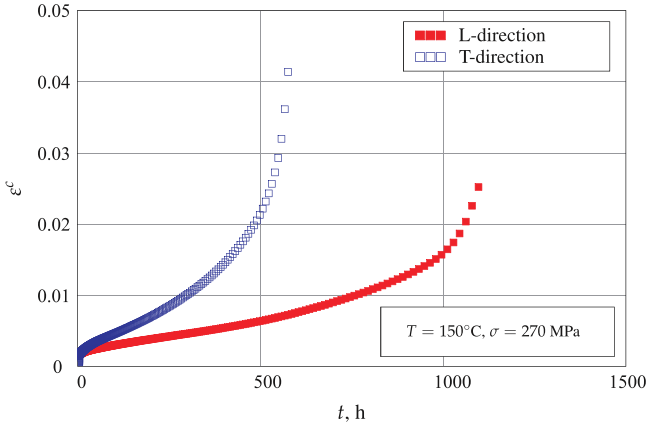

Fig. 4. Creep rate vs. time curves for longitudinal and transverse directions of AA2014 for T=150 °C and σ=270 MPa.

creep rates over the entire time of testing. From creep rate vs. creep strain curves the minimum creep rates were obtained. Fig. 2 shows normalized minimum creep rates vs. normalized stress obtained from creep curves for longitudinal and transverse specimen.

To normalize the data the Arrhenius function of the temperature

$$f(T) = \exp\left(-\frac{Q}{RT}\right) \tag{1}$$

with apparent activation energy Q, the universal gas constant R and absolute temperature T is applied. The obtained value Q=175.42 kJ/mol is consistent with the data published in [4]. The reference stress $\sigma_0 = 320$ MPa is introduced to split the ranges of power law creep and power law breakdown, as shown in Fig. 2. According to experimental data presented in Fig. 2 the anisotropy is primarily observable in the power law range. Here the creep rate in the T direction is 2.43 times higher that the creep rate in the L direction for the same stress level. In the power law breakdown regime the corresponding ratio of creep rates takes the value is within the range 1.1–1.5 depending on the stress level. Such the difference between L and T data is not essential, if compared to the usual scatter of experimental data in the creep range, and can be neglected.

Fig. 3 shows the creep rate vs. time curves for transverse specimen for T=150 °C and different stress levels.

It can be observed that the material does not exhibit the pronounced secondary creep stage. On the contrary, the creep rate decreases at the beginning, attains a minimum value and increases up to the final failure. The tertiary creep stage is controlled by several processes including the ageing of the strengthening θ' phase, formation of voids on blocky shaped particles as well as cross section shrinkage of specimen as a result of excessive elongation at high stress levels.

Creep strain vs. time curves for longitudinal and transverse specimen are presented in Fig. 4. The data show that transverse specimen exhibit the higher creep rate, the higher creep ductility and the shorter creep life for the same stress and the temperature level.

3. Constitutive models

3.1. Stress state decomposition and a model for minimum creep rates

In what follows let us assume that the minimum creep rates in R and T directions are approximately the same and the plane spanned on R and T directions to be the isotropy plane. Constitutive equations

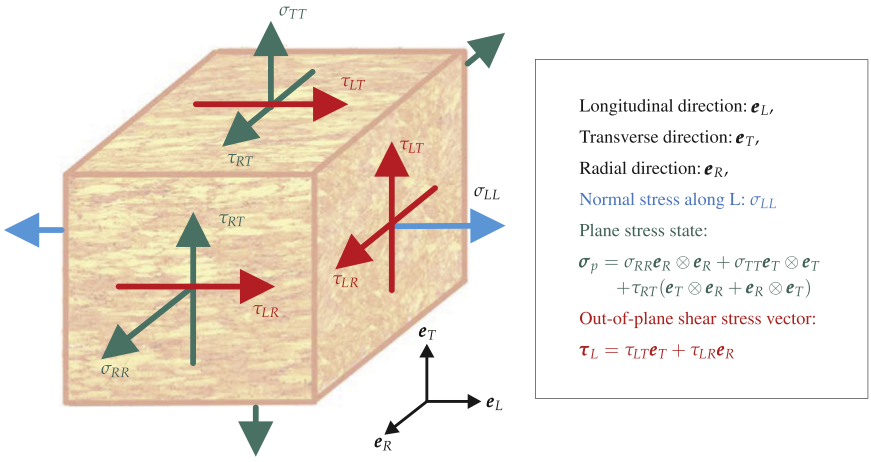

Fig. 5. Stress state decomposition.

of transversally-isotropic steady-state creep were applied in [18] to modeling deep drawing sheets and in [20] to characterize multi-pass weld metals, for example.

Let $\boldsymbol{e}_L$ be the unit vector that designates the direction L, $\boldsymbol{I}$ the second rank unit tensor and $\boldsymbol{P} = \boldsymbol{I} - \boldsymbol{e}_L \otimes \boldsymbol{e}_L$ the projector onto the RT plane. For anisotropic materials different parts of the stress state cause different creep responses. Therefore let us decompose the stress state characterized by the stress tensor $\boldsymbol{\sigma}$ into the three parts including the tension (compression) along L σ_{LL}, the plane stress state in the RT-plane $\boldsymbol{\sigma}_p$ and the out of plane shear characterized by the shear stress vector $\boldsymbol{\tau}_L$. Fig. 5 illustrates the corresponding components of the stress tensor. The decomposition has the following form

$$\boldsymbol{\sigma} = \sigma_{LL}\boldsymbol{e}_L \otimes \boldsymbol{e}_L + \boldsymbol{\sigma}_p + \boldsymbol{\tau}_L \otimes \boldsymbol{e}_L + \boldsymbol{e}_L \otimes \boldsymbol{\tau}_L \tag{2}$$

By subtracting the hydrostatic stress state the stress deviator $\boldsymbol{s}$ can be given as follows

$$\boldsymbol{s} = \boldsymbol{s}_L + \boldsymbol{s}_p + \boldsymbol{\tau}_L \otimes \boldsymbol{e}_L + \boldsymbol{e}_L \otimes \boldsymbol{\tau}_L, \tag{3}$$

where

$$\boldsymbol{s}_L = \left(\sigma_{LL} - \frac{1}{2}\mathrm{tr}\boldsymbol{\sigma}_p\right)\left(\boldsymbol{e}_L \otimes \boldsymbol{e}_L - \frac{1}{3}\boldsymbol{I}\right), \quad \boldsymbol{s}_p = \boldsymbol{\sigma}_p - \frac{1}{2}\mathrm{tr}\boldsymbol{\sigma}_p(\boldsymbol{I} - \boldsymbol{e}_L \otimes \boldsymbol{e}_L) \tag{4}$$

With the decomposition (3), the creep potential hypothesis and the assumption that the volumetric creep rate is negligible, the constitutive equation can be formulated as follows [18,17]

$$\dot{\boldsymbol{\varepsilon}}^c = \frac{3}{2}\dot{\varepsilon}_0 f(T)\left(\frac{\sigma_{eq}}{\sigma_0}\right)^n \frac{1}{\sigma_{eq}}\left[\alpha_1\boldsymbol{s}_L + \alpha_2\boldsymbol{s}_p + \alpha_3(\boldsymbol{\tau}_L \otimes \boldsymbol{e}_L + e_L \otimes \boldsymbol{\tau}_L)\right], \tag{5}$$

where $\boldsymbol{\varepsilon}^c$ is the tensor of inelastic strains, $\dot{\varepsilon}_0$, σ_0, n and α_i, $i = 1,2,3$ are material parameters. The equivalent stress σ_{eq} is defined as follows

$$\sigma_{eq}^2 = \frac{3}{2}\left(\alpha_1\mathrm{tr}\boldsymbol{s}_L^2 + \alpha_2\mathrm{tr}\boldsymbol{s}_p^2 + 2\alpha_3\boldsymbol{\tau}_L \cdot \boldsymbol{\tau}_L\right) \tag{6}$$

To identify the material parameters families of creep curves for different stress levels for three independent kinds of loading are required. These include the loading in L and T directions, respectively as well as any kind of loading that leads to non-zero out-of-plane shear stress. For $\alpha_1 = \alpha_2 = \alpha_3 = 1$ the von Mises equivalent stress follows from Eq. (6). Equation (5) reduces to the Norton-Bailey-Odqvist equation of isotropic creep in the power law range [21].

For the tensile stress σ_{LL} the longitudinal creep rate $\dot{\varepsilon}^c_{\mathrm{TT}}$ can be computed from Eq. (5) as follows

$$\dot{\varepsilon}^c_{\mathrm{LL}} = \dot{\varepsilon}_0 f(T)\left(\frac{\sigma_{LL}}{\sigma_0}\right)^n \alpha_1^{\frac{n+1}{2}} \tag{7}$$

The creep rate in the transverse direction for the applied stress σ_{TT} is

$$\dot{\varepsilon}^c_{\mathrm{TT}} = \dot{\varepsilon}_0 f(T)\left(\frac{\sigma_{TT}}{\sigma_0}\right)^n \left(\frac{\alpha_1 + 3\alpha_2}{4}\right)^{\frac{n+1}{2}} \tag{8}$$

The function $f(T)$ and the parameter $\dot{\varepsilon}_0$ can be identified from minimum creep rate vs. stress data generated from transverse creep curves, Fig. 2. In this case the parameter α_2 can be set to one. To identify the parameter α_1 the ratio of creep rates α for the same stress level can be computed from Eqs. (7) and (8) as follows

$$\alpha = \frac{\dot{\varepsilon}^c_{\mathrm{TT}}}{\dot{\varepsilon}^c_{\mathrm{LL}}} = \left(\frac{\alpha_1 + 3}{4\alpha_1}\right)^{\frac{n+1}{2}} \tag{9}$$

For the given values of $\alpha$and n, Fig. 2, the solution of Eq. (9) is $\alpha_1 = 0.81$.

The constitutive model (5) is available in commercial finite element codes and can be used for the structural analysis. One limitation is the assumption of the steady-state creep process. Primary creep and creep transients for the rapid loading changes as well as tertiary creep due to overageing and damage are not considered. Although approaches are proposed to generalize the anisotropic equation (5) by introduction of tensorial state variables [5], experimental data to identify the large number of material properties is hardy available. Let us note that additional assumptions are required, to identify the parameter α_3 in Eq. (6), since corresponding experimental data, e.g. creep curves under torsion, are missing.

3.2. Phase mixture model

To develop an alternative model let us analyze the origins of anisotropic creep for the considered alloy. The following microstructural features can be responsible for the observed direction-dependent creep:

- Crystallographic texture induced by processing
- θ' particles oriented on specific crystallographic planes
- Elongated grains and grain boundaries

Anisotropic creep properties due to texture and particle orientation effects are documented for many alloys over a wide range of stress and temperature [18]. From the theoretical point of view the greatest influence of texture and oriented particles is expected in the power law breakdown regime where the deformation is primarily controlled by glide processes in well-defined crystallographic slip planes and diffusion controlled climb processes are

not essential [22]. In this regime the influence of texture can also be analyzed within the crystal viscoplasticity theory by estimation of creep rates for single crystals and isotropic polycrystals [23].

For low and moderate stress values and longer test durations grain boundary deformation mechanisms, e.g. diffusion creep and grain boundary sliding have significant influence on the overall creep process [22,24,25]. For the loading in L direction a stress redistribution between grain interiors and grain boundary regions is expected as a result of different creep rates in different microstructural zones. On the other hand no essential changes in the microstructural stress state can be assumed if the material is loaded in T direction. As a result the difference in the overall creep rates are observed – T specimen exhibit higher creep rates than L specimen for the same overall stress level in the power law creep regime.

Experimental data for the considered alloy show that the ratio of minimum creep rates in T and L directions in the power law breakdown regime is in the range of 1.1–1.5. This anisotropy can be attributed to the texture and particle orientation. In the power law creep regime the ratio is significantly higher with the value of 2.43. This indicates that the anisotropy is primarily due to elongated grains and grain boundaries. In what follows constitutive equations of creep within the power law regime will be developed. For the sake of simplicity, texture and particle orientation effects will be ignored.

To account for the heterogeneous deformation on the microscale various approaches were recently developed. They include the micropolar, micromorphic, gradient and other enhanced theories of plasticity, e.g. [26–28]. In this paper we follow and extend the phase mixture (composite) approach as discussed in materials science [29,30] and continuum mechanics [6,31]. To this end we consider a composite with two constituents having different creep properties. The first constituent is related to the grain interior while the second one corresponds to grain boundary regions. In the following derivations we use the subscript A for grain interiors and B for grain boundary regions, respectively.

The constitutive equations include the elasticity laws for the constituents

$$\boldsymbol{s}_k = 2G(\boldsymbol{\epsilon}_k - \boldsymbol{\epsilon}_k^c), \quad \sigma_{H_k} = K\varepsilon_{V_k}, \quad k = \mathrm{A, B}, \tag{10}$$

where $\boldsymbol{s}_k$ is the stress deviator, $\boldsymbol{\epsilon}_k$ strain deviator, $\boldsymbol{\epsilon}_k^c$ inelastic strain deviator, σ_{H_k} hydrostatic stress and ε_{V_k} is the volumetric strain of the k-th constituent. G is the shear modulus and K is the bulk modulus. The rate equations for the inelastic strain deviators $\boldsymbol{\epsilon}_k^c$ are assumed as follows

$$\dot{\boldsymbol{\epsilon}}_k^c = \frac{3}{2}\dot{\varepsilon}_{\mathrm{vM}_k}\frac{\boldsymbol{s}_k}{\sigma_{\mathrm{vM}_k}}, \quad k = \mathrm{A, B}, \tag{11}$$

where the von Mises equivalent stress σ_{vM_k} and the von Mises equivalent strain rate $\dot{\varepsilon}_{\mathrm{vM}_k}$ are defined as follows

$$\sigma_{\mathrm{vM}_k}^2 = \frac{3}{2}\mathrm{tr}\boldsymbol{s}_k^2, \quad \dot{\varepsilon}_{\mathrm{vM}_k}^2 = \frac{2}{3}\mathrm{tr}(\dot{\boldsymbol{\epsilon}}_k^c)^2 \tag{12}$$

The stress tensor and the strain tensor of the composite are defined by the mixture rules as follows

$$\boldsymbol{\sigma} = \nu_\mathrm{A}\boldsymbol{\sigma}_\mathrm{A} + \nu_\mathrm{B}\boldsymbol{\sigma}_\mathrm{B}, \quad \boldsymbol{\varepsilon} = \nu_\mathrm{A}\boldsymbol{\varepsilon}_\mathrm{A} + \nu_\mathrm{B}\boldsymbol{\varepsilon}_\mathrm{B}, \quad \nu_\mathrm{A} + \nu_\mathrm{B} = 1, \tag{13}$$

where ν_k is the volume fraction of the k-th constituent. From Eqs. (13) and (10) the rules for the for deviatoric parts of stress and strain states as well as for inelastic parts of strain tensors can be derived as follows

$$\boldsymbol{s} = \nu_\mathrm{A}\boldsymbol{s}_\mathrm{A} + \nu_\mathrm{B}\boldsymbol{s}_\mathrm{B}, \quad \boldsymbol{\epsilon} = \nu_\mathrm{A}\boldsymbol{\epsilon}_\mathrm{A} + \nu_\mathrm{B}\boldsymbol{\epsilon}_\mathrm{B}, \quad \boldsymbol{\epsilon}^c = \nu_\mathrm{A}\boldsymbol{\epsilon}_\mathrm{A}^c + \nu_\mathrm{B}\boldsymbol{\epsilon}_\mathrm{B}^c \tag{14}$$

An essential ingredient of any phase mixture model is a rule for the interaction between the constituents. One possibility is the iso-strain approach as proposed in [29,30] and [6] to develop creep models of several isotropic materials. To capture anisotropic creep let us apply the following interaction rule

$$\boldsymbol{\Delta} = \boldsymbol{\Delta}^c - \frac{3}{2}\Delta_{LL}^c\left(\boldsymbol{e}_L \otimes \boldsymbol{e}_L - \frac{1}{3}\boldsymbol{I}\right), \tag{15}$$

with

$$\boldsymbol{\Delta} = \boldsymbol{\varepsilon}_\mathrm{B} - \boldsymbol{\varepsilon}_\mathrm{A}, \quad \boldsymbol{\Delta}^c = \boldsymbol{\epsilon}_\mathrm{B}^c - \boldsymbol{\epsilon}_\mathrm{A}^c, \quad \Delta_{LL}^c = \epsilon_{LL_\mathrm{B}}^c - \epsilon_{LL_\mathrm{A}}^c$$

From Eq. (15) the iso-strain (Voigt-type) rule for the longitudinal strains ε_{LL_k} and volumetric strains can be obtained

$$\varepsilon_{LL_\mathrm{A}} = \varepsilon_{LL_\mathrm{A}} = \varepsilon_{LL}, \quad \varepsilon_{V_\mathrm{A}} = \varepsilon_{V_\mathrm{A}} = \varepsilon_V \tag{16}$$

With Eqs. (10) and (15) the difference in stress deviators $\boldsymbol{s}_\Delta = \boldsymbol{s}_\mathrm{B} - \boldsymbol{s}_\mathrm{A}$ can be computed as follows

$$\boldsymbol{s}_\Delta = -3G\Delta_{LL}^c\left(\boldsymbol{e}_L \otimes \boldsymbol{e}_L - \frac{1}{3}\boldsymbol{I}\right) \tag{17}$$

From Eq. (17) the iso-stress (Reuss-type) rules for the plane deviatoric stress states $\boldsymbol{s}_{p_k}$ and the out-of-plane shear stress vectors $\boldsymbol{\tau}_{L_k}$ follow

$$\boldsymbol{s}_{p_\mathrm{A}} = \boldsymbol{s}_{p_\mathrm{B}} = \boldsymbol{s}_p, \quad \boldsymbol{\tau}_{L_\mathrm{A}} = \boldsymbol{\tau}_{L_\mathrm{B}} = \boldsymbol{\tau}_L \tag{18}$$

Since the bulk moduli of the constituents are assumed to be the same, Eqs. (10) and (16) provide the equality of hydrostatic stresses

$$\sigma_{H_\mathrm{A}} = \sigma_{H_\mathrm{A}} = \sigma_H$$

To complete the model the von Mises equivalent creep rate for each phase should be specified as a function of the corresponding von Mises equivalent stress, temperature and a set of internal state variables to characterize changes in microstructure.

The constitutive equation for the matrix material is formulated as proposed in [32]

$$\dot{\varepsilon}_{\mathrm{vM}_\mathrm{A}} = a_0 f_0(T)\left(\frac{\sigma_{\mathrm{vM}_\mathrm{A}}}{\hat{\sigma}}\right)^n, \tag{19}$$

where a_0 is the material property and

$$f_0(T) = \exp\left(-\frac{Q_0}{RT}\right) \tag{20}$$

Let us note that the activation energy Q_0 differs from the corresponding quantity given in Eq. (1) for the minimum creep rates. Following [32] the drag stress $\hat{\sigma}$ can be given as a superposition of the dislocation density and the particle hardening contributions as follows

$$\hat{\sigma} = MGb\left(\zeta\sqrt{\rho} + \chi\frac{1}{D}\right), \tag{21}$$

where M is the Taylor factor, b is the magnitude of the Burgers vector, ρ is the mean dislocation density and D is the mean characteristic size of particles. ζ and χ are weighting factors characterizing the contribution of Taylor-type hardening due to dislocations and Orowan-type hardening due to the presence of θ' phase. According to Eq. (21) the presence of particles influences the drag stress and consequently the creep rate. The particle hardening drag stress value is usually lower than the Orowan stress. This is explained by a variety of dislocation-particle interaction mechanisms operating in the creep range, e.g. dislocation climb over particles [33]. Furthermore, in the creep range the presence of particles has an influence on both the storage/immobilization of dislocations and dynamic recovery processes. To characterize the evolution of the dislocation structure let us extend the exponential type kinetic equation, proposed in [29], to account for the influence of particles as follows

$$\dot{X} = C(X_* - X)\dot{\varepsilon}_{\mathrm{vM}_\mathrm{A}}, \quad X = \sqrt{\frac{\rho}{\rho_0}}, \quad X_* = X_\infty\frac{D_0}{D} \tag{22}$$

where C is a constant, ρ_0 is a reference dislocation density, D_0 is a reference characteristic size of particles and X_∞ is a function of

stress and temperature. According to Eq. (22) the particle coarsening lowers the saturated dislocation density X_* and contributes to material softening.

The microstructural stability of age-hardenable Al alloys depends essentially on the precipitation sequences. For the considered alloy the high temperature exposure of the matrix is related to the completion of precipitation of θ' particles [4]. The coarsening of θ' particles is governed by the mass transport processes associated with the diffusion of Cu in Al. In [4] the following equation for the mean particle size is utilized

$$D^m = D_0^m + K(T)t, \quad K(T) = K_0 \exp\left(\frac{-Q_{\mathrm{Cu}}}{RT}\right), \quad m = 2 \tag{23}$$

where K_0 is a material property and Q_{Cu} is the activation energy for diffusion of Cu in Al. One feature of Eq. (23) is the coarsening index m which takes the value 2 for rod-like particles. Following [34] let us introduce the internal state variable $\Phi = D_0/D$. From Eq. (23) the following kinetic equation can be derived

$$\dot{\Phi} = -\frac{A_s}{m}\Phi^{m+1}, \quad A_s(T) = A_0 \exp\left(\frac{-Q_{\mathrm{Cu}}}{RT}\right), \quad A_0 = \frac{K_0}{D_0^m} \tag{24}$$

For the von Mises equivalent creep rate of the phase B let us apply the following constitutive equation

$$\dot{\varepsilon}_{\mathrm{vM_B}} = \dot{\varepsilon}_{\mathrm{vM_A}} \frac{\sigma_{\mathrm{vM_B}}}{\sigma_{\mathrm{vM}}} \frac{1}{g}, \tag{25}$$

with g is a function of the von Mises equivalent stress.

3.3. Reduced model

For the stable identification as well as for the use in structural analysis the phase mixture model should be reduced to a set of kinetic equations with respect to the macroscopic variables. To accomplish this let us introduce the backstress deviator $\boldsymbol{\beta}$ and the active stress deviator $\bar{\boldsymbol{s}}$ as follows

$$\boldsymbol{\beta} = \nu_{\mathrm{B}}(\boldsymbol{s}_{\mathrm{B}} - \boldsymbol{s}_{\mathrm{A}}), \quad \bar{\boldsymbol{s}} = \boldsymbol{s} - \boldsymbol{\beta} \tag{26}$$

Furthermore let us assume that the creep rate of the composite is primarily determined by the creep rate of grain interiors

$$\dot{\boldsymbol{\varepsilon}}^c \approx \nu_{\mathrm{A}} \dot{\boldsymbol{\varepsilon}}_{\mathrm{A}}^c \tag{27}$$

From Eqs. (10)–(18), (25), (26) and (27) the following constitutive and evolution equation can be obtained

$$\dot{\boldsymbol{\varepsilon}}^c = \frac{3}{2}\dot{\varepsilon}_{\mathrm{vM}}\frac{\bar{\boldsymbol{s}}}{\bar{\sigma}_{\mathrm{vM}}}, \quad \bar{\sigma}_{\mathrm{vM}}^2 = \frac{3}{2}\mathrm{tr}\bar{\boldsymbol{s}}^2, \quad \boldsymbol{\beta} = \beta\left(\boldsymbol{e}_L \otimes \boldsymbol{e}_L - \frac{1}{3}\boldsymbol{I}\right),$$
$$\dot{\beta} = C_\beta\left(\dot{\varepsilon}_{LL}^c - \dot{\varepsilon}_{\mathrm{vM}}\frac{\beta}{h_\infty \sigma_{\mathrm{vM}}}\right), \tag{28}$$

where

$$C_\beta = 3\frac{\nu_{\mathrm{B}}}{\nu_{\mathrm{A}}}G, \quad h_\infty = \frac{\nu_{\mathrm{B}}}{\nu_{\mathrm{A}}}g$$

Further reductions can be accomplished by introducing the new hardening variable H as follows

$$H = \frac{X + \mu\Phi}{(1+\mu)\Phi}, \quad \mu = \frac{\chi}{\zeta}\frac{1}{D_0\sqrt{\rho_0}} \tag{29}$$

With Eqs. (27) and (29) the constitutive equation (19) takes the form

$$\dot{\varepsilon}_{\mathrm{vM}} = \dot{\varepsilon}_0 f_0(T)\left(\frac{\bar{\sigma}_{\mathrm{vM}}}{\sigma_0}\frac{1}{H\Phi}\right)^n, \quad \frac{\dot{\varepsilon}_0}{\sigma_0^n} = a_0\nu_{\mathrm{A}}MGb\zeta\sqrt{\rho_0}(1+\mu) \tag{30}$$

From Eqs. (22), (24) and (27) the following evolution equation for the hardening variable H can be derived

$$\dot{H} = C_H(H_\infty - H)\dot{\varepsilon}_{\mathrm{vM}}, \quad C_H = \frac{C}{\nu_{\mathrm{A}}}, \quad H_\infty = \frac{X_\infty + \mu}{1+\mu} \tag{31}$$

4. Identification

4.1. Summary of constitutive and evolution equations

Let us summarize the introduced constitutive model as well as material properties to be identified from experimental data. With Eqs. (28) and (30) the constitutive equation for the creep rate tensor takes the form

$$\dot{\boldsymbol{\varepsilon}}^c = \frac{3}{2}\dot{\varepsilon}_0 f_0(T)\left(\frac{\bar{\sigma}_{\mathrm{vM}}}{\sigma_0}\frac{1}{H\Phi}\right)^n \frac{\bar{\boldsymbol{s}}}{\bar{\sigma}_{\mathrm{vM}}}, \quad \bar{\sigma}_{\mathrm{vM}}^2 = \frac{3}{2}\mathrm{tr}\bar{\boldsymbol{s}}^2, \quad \bar{\boldsymbol{s}} = \boldsymbol{s} - \boldsymbol{\beta} \tag{32}$$

According to Eq. (32) the creep rate is controlled by three state variables including the backstress deviator $\boldsymbol{\beta}$, the scalar hardening variable H and the overageing variable Φ. The backstress deviator characterizes the microstress state in the phase mixture due to different deformation rates in grains and grain boundary regions. It takes into account the anisotropy due to elongated grains. The corresponding evolution equation is derived from the composite model as follows

$$\boldsymbol{\beta} = \beta\left(\boldsymbol{e}_L \otimes \boldsymbol{e}_L - \frac{1}{3}\boldsymbol{I}\right), \quad \dot{\beta} = C_\beta\left(\dot{\varepsilon}_{LL}^c - \dot{\varepsilon}_{\mathrm{vM}}\frac{\beta}{h_\infty\sigma_{\mathrm{vM}}}\right) \tag{33}$$

The variable H defined by Eq. (29) combines the state of dislocation microstructure and the θ' phase. The hardening/recovery type evolution equation is

$$\dot{H} = C_H(H_\infty - H)\dot{\varepsilon}_{\mathrm{vM}} \tag{34}$$

The variable Φ characterizes the overageing state of the θ' phase. The corresponding evolution equation has the form

$$\dot{\Phi} = -\frac{A_s}{m}\Phi^{m+1} \tag{35}$$

Eqs. (32)–(35) include the material parameters $\dot{\varepsilon}_0$, σ_0, n, C_H, m, the functions of temperature f_0, C_β and A_s as well as the functions of stress H_∞ and h_∞. The constitutive equation (32) can only be applied for the power law creep regime. Within this regime h_∞ is usually assumed to be constant. Let us note that advanced response functions of stress and temperature might be required to capture inelastic behavior in both power law and power law breakdown regimes [7].

To develop a robust identification procedure explicit expressions for the creep rate as a function of the creep strain and/or time for a constant uni-axial stress and temperature should be given. In what follows we derive such functions from Eqs. (32)–(35) for constant tensile stress in L and T directions.

4.2. Longitudinal direction

With the constant tensile stress σ_{LL} applied in L direction the stress tensor, the stress deviator the von Mises equivalent stress and the active von Mises equivalent stress are

$$\boldsymbol{\sigma} = \sigma_{LL}\boldsymbol{e}_L \otimes \boldsymbol{e}_L, \quad \boldsymbol{s} = \sigma_{LL}\left(\boldsymbol{e}_L \otimes \boldsymbol{e}_L - \frac{1}{3}\boldsymbol{I}\right), \quad \sigma_{\mathrm{vM}} = \sigma_{LL}, \quad \bar{\sigma}_{\mathrm{vM}} = \sigma_{LL} - \beta \tag{36}$$

The constitutive equation for the creep rate in L direction is derived from Eq. (32) as follows

$$\dot{\varepsilon}_{LL}^c = \dot{\varepsilon}_{\mathrm{vM}} = \dot{\varepsilon}_0 f_0(T)\left(\frac{\sigma_{LL} - \beta}{\sigma_0 H\Phi}\right)^n \tag{37}$$

The evolution Eqs. (33) and (34) take the form

$$\dot{\beta} = C_\beta\dot{\varepsilon}_{LL}^c\left(1 - \frac{\beta}{h_\infty\sigma_{LL}}\right), \quad \dot{H} = C_H(H_\infty - H)\dot{\varepsilon}_{LL}^c \tag{38}$$

Integration of Eqs. (38) yields the backstress and the hardening variable as functions of the longitudinal creep strain

$$\beta = h_\infty \sigma_{LL}\left[1-\exp\left(-\frac{C_\beta}{h_\infty \sigma_{LL}}\varepsilon^c_{LL}\right)\right], \quad H = H_\infty - (H_\infty - 1)\exp(-C_H\varepsilon^c_{LL}) \tag{39}$$

Integration of Eq. (35) provides the ageing variable within the time interval $[0,t]$

$$\Phi = (1+A_s t)^{-1/m} \tag{40}$$

Inserting expressions for internal state variables (39) and (40) into Eq. (37) provides the longitudinal creep rate as a function of stress, temperature, creep strain and time

$$\dot\varepsilon^c_{LL} = \dot\varepsilon_0 f_0(T)\left(\frac{\sigma_{LL}}{\sigma_0}\right)^n \left[\frac{1-h_\infty+h_\infty\exp\left(-\frac{C_\beta}{h_\infty\sigma_{LL}}\varepsilon^c_{LL}\right)}{H_\infty-(H_\infty-1)\exp(-C_H\varepsilon^c_{LL})}\right]^n [1+A_s(T)t]^{n/m} \tag{41}$$

4.3. Transverse direction

With the applied tensile stress σ_{TT} the stress tensor, its deviatoric part, the von Mises equivalent stress and the active von Mises equivalent stress are

$$\boldsymbol{\sigma} = \sigma_{TT}\boldsymbol{e}_T\otimes\boldsymbol{e}_T, \quad \boldsymbol{s} = \sigma_{TT}\left(\boldsymbol{e}_T\otimes\boldsymbol{e}_T-\frac{1}{3}\boldsymbol{I}\right), \quad \sigma_{\mathrm{vM}} = \sigma_{TT},$$

$$\overline{\sigma}_{\mathrm{vM}} = \sqrt{\sigma^2_{TT}+\sigma_{TT}\beta+\beta^2} \tag{42}$$

The constitutive equation for the creep rate in T direction follows from Eq. (32)

$$\dot\varepsilon^c_{TT} = \dot\varepsilon_0 f_0(T)\left(\frac{\sqrt{\sigma^2_{TT}+\sigma_{TT}\beta+\beta^2}}{\sigma_0 H\Phi}\right)^{n-1}\frac{\sigma_{TT}+\beta/2}{\sigma_0 H\Phi} \tag{43}$$

The evolution equation (33) takes the form

$$\dot\beta = -C_\beta\dot\varepsilon^c_{TT}\frac{\sigma_{TT}+2\beta}{2\sigma_{TT}+\beta}\left(1+2\frac{\sqrt{\sigma^2_{TT}+\sigma_{TT}\beta+\beta^2}}{\sigma_{TT}+2\beta}\frac{\beta}{h_\infty\sigma_{TT}}\right) \tag{44}$$

The evolution equation (34) can be specified as follows

$$\dot H = C_H(H_\infty - H)\dot\varepsilon^c_{TT}\frac{\sqrt{\sigma^2_{TT}+\sigma_{TT}\beta+\beta^2}}{\sigma_{TT}+\beta/2} \tag{45}$$

The approximate analytical solution to Eq. (44) is

$$\beta = -h_T\sigma_{TT}\left[1-\exp\left(-\frac{C_\beta}{2h_T\sigma_{TT}}\varepsilon^c_{TT}\right)\right], \quad h_T = \frac{2h_\infty}{4+3h_\infty} \tag{46}$$

The backstress saturation parameter h_∞ must be identified from the longitudinal creep curves and takes the values in the range $0\le h_\infty\le 1$. From Eq. (46) it follows that the backstress saturation parameter for the transverse direction is in the range $0\le h_T\le 2/7$ such that $|\beta|<2/7\sigma_{TT}$. Therefore, the backstress evolution has a minor influence on the creep process for loading in T direction. The creep behavior of the phase mixture is determined by the creep rate of grain interiors and the stress redistribution between the phases is not essential. For the identification the backstress can be set to zero such that the expression for creep rate takes the following simplified form

$$\dot\varepsilon^c_{TT} = \dot\varepsilon_0 f_0(T)\left(\frac{\sigma_{TT}}{\sigma_0}\right)^n\left[\frac{1}{H_\infty-(H_\infty-1)\exp(-C_H\varepsilon^c_{TT})}\right]^n [1+A_s(T)t]^{n/m} \tag{47}$$

4.4. Identification procedure

To find the material parameters in the constitutive and evolution equations the following step-by-step identification procedure is performed:

- Experimental creep curves (creep strain vs. time curves) are smoothed and transformed to the creep rate vs. creep strain curves and creep rate vs. time curves
- Minimum strain rates as functions of stress and temperature are processed from experimental data
- The creep exponent in the power law creep regime is determined from the minimum creep rate vs. stress dependencies
- The overageing process of the considered alloy is discussed in detail in [4], where the material parameters in Eq. (23) are identified as follows

  $K_0 = 4.44\cdot 10^{-5}\ \mathrm{m^2/s}, \quad Q_{\mathrm{Cu}} = 133.9\ \mathrm{kJ/mol}$

  The characteristic size of the particles ranges between 0.05 μm and 0.1 μm [19,35]. Therefore, the bounds for the property A_0 can be estimated by Eq. (24)
- With experimental data for creep rates under transverse loading and Eq. (47) the material properties $\dot\varepsilon_0$, σ_0, C_H, A_0 as well as functions f_0 and H_∞ are identified by the least square method
- With experimental data from longitudinal tests and Eq. (41) the material properties C_β and h_∞ are identified by the least square method.

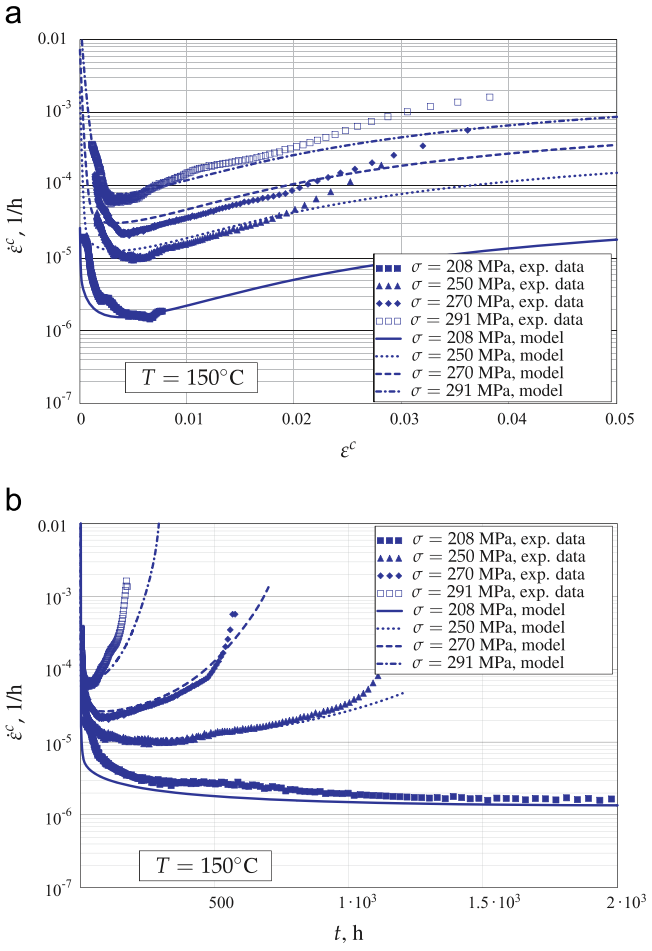

Fig. 6. Experimental data and model predictions for T direction at $T=150$ °C and different stress levels. (a) Creep rate vs. creep strain, (b) creep rate vs. time.

To verify the results of the identification procedure Eqs. (32)–(35) are solved numerically for longitudinal and transverse loadings and the results are compared with experimental data.

Fig. 6 shows results of identification for T direction at constant temperature $T=150\ ^{\circ}\mathrm{C}$ and different stress levels.

Let us note that the backstress has minor influence on the creep response for the loading in T direction. The creep rate vs. creep stain, Fig. 6(a) and creep rate vs. time curves, Fig. 6(b) are well reproduced by the developed model with two scalar state variables H and Φ. A slight disagreement between the experimental data and the model is observed in the final stage of the creep curves before the fracture. Here the experimental creep rates are higher than the creep rates predicted by the model. One way to improve the model is the use of an additional damage state variable and damage evolution equation.

Fig. 7 shows experimental data and results of identification for L direction. Here only parameters in the backstress evolution equation were identified from experimental data while equations for the variables H and Φ were calibrated against creep curves for T direction previously.

As the results show the backstress together with the hardening variable H describes well the primary creep stage up to the minimum creep rates. This confirms that the proposed phase mixture model is well suitable to reflect anisotropic effects of inelastic deformation. However, the introduced ageing variable cannot accurately capture the tertiary creep stage for the loading in L direction. The experimental creep rates are higher than creep rates predicted by the model in the most part of the tertiary creep stage. This disagreement indicates that damage processes control the tertiary creep rate and are mostly observable for the loading in L direction. The essential creep cavitation of L specimen was documented in [3].

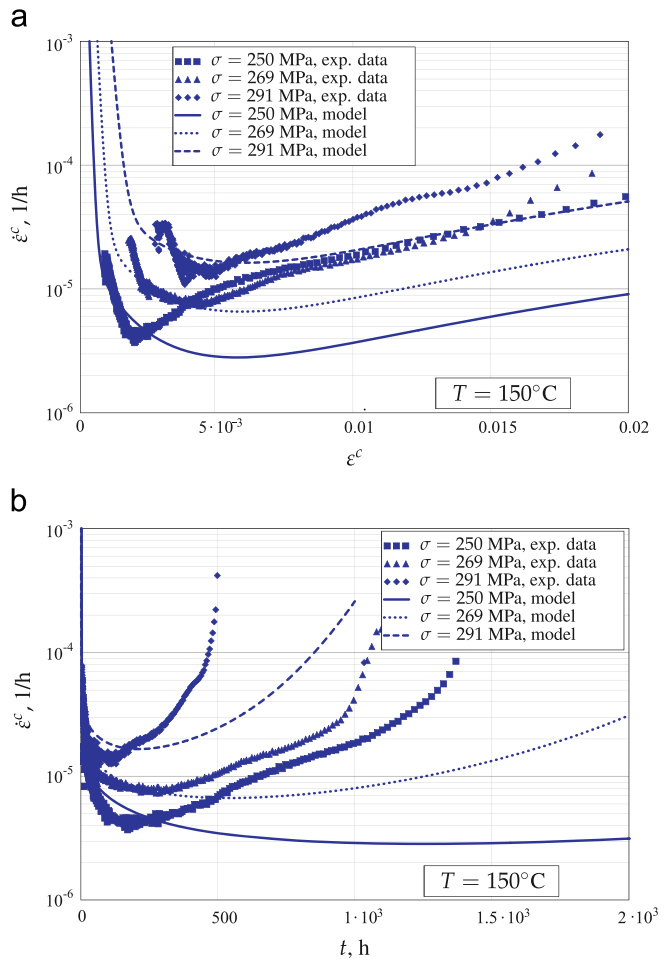

Fig. 7. Experimental data and model predictions for L direction at $T=150\ ^{\circ}\mathrm{C}$ and different stress levels. (a) Creep rate vs. creep strain, (b) creep rate vs. time.

Let us give a summary of identified material parameters in Eqs. (32)–(35) for $T=150\ ^{\circ}\mathrm{C}$

$$\dot{\varepsilon}_0 f_0(T) = 907.4\ 1/\mathrm{h}, \quad \sigma_0 = 320\ \mathrm{MPa} \quad n = 9.94,$$

$$H_\infty(\sigma_{\mathrm{vM}}) = H_0\left(\frac{\sigma_{\mathrm{vM}}}{\sigma_0}\right)^{-k}, \quad H_0 = 5.76, \quad k = 5.91, \quad C_H = 182,$$

$$A_s(T) = 0.0308\ 1/\mathrm{h}, \quad m = 2,$$

$$h_\infty = 0.585, \quad C_\beta = 6.37\cdot10^4\ \mathrm{MPa}$$

5. Conclusions and recommendations

The aim of this paper was to analyze microstructural processes that lead to anisotropic behavior of forged aluminium alloy AA2014 and to develop a constitutive model for the creep behavior under multi-axial stress state.

Based on the results we may conclude as follows:

- The principal origin of the anisotropic creep could be explained on the basis of a composite structure made from elongated grains and grain boundary regions
- The phase mixture approach with the anisotropic interaction rule is applicable to model directionally dependent stress redistributions for materials with elongated grains
- The proposed model can be reduced to a set of equations with three internal state variables: the backstress, the dislocation density hardening variable and the particle overageing variable. With such a formulation the material parameters can be identified from creep curves for two loading directions
- The introduced ageing variable and corresponding kinetic equation describe tertiary creep stage accurately only for T direction. To capture accelerated creep in L direction an additional damage state variable is required.

The developed model is able reflect basic features of anisotropic creep deformation for forged AA2014 alloy and can also be applied for other alloys having microstructure with elongated grains. It can be utilized inside any commercial finite element code for the use in structural analysis.

The approach is limited to the power law creep range which is the case for many industrial applications of forged aluminium components serviced by intermediate temperatures. The model can be extended to capture both the power law and power law breakdown ranges by introduction of appropriate response functions of stress. This would require the use of advanced identification techniques [7]. Furthermore, texture and particle orientation effects should be included in the future on the basis of crystal viscoplasticity modeling and experimental data for distribution of crystallographic orientations. To validate the model additional data from independent creep tests are required. One way is to compare the model predictions with experimental data for notched specimen. Furthermore, creep damage processes should be considered to predict the life-time of specimen and components. To this end an appropriate tensor-valued damage variable and evolution equation should be introduced. For isotropic materials approaches exist to consider directionally dependent creep cavitation, e.g. [36]. Further investigations are required to formulate and identify anisotropic damage processes for initially anisotropic materials like forged aluminum alloys.

References

[1] I.J. Polmear, JIM, Materials Transactions 37 (1996) 12–31.
[2] I.J. Polmear, Materials Forum 28 (2004) 1–14.
[3] E. Gariboldi, A. Conte, Advanced Materials Modelling for Structures, Springer, 2013, pp. 165–175.
[4] E. Gariboldi, F. Casaro, Materials Science and Engineering: A 462 (2007) 384–388.
[5] J.L. Chaboche, International Journal of Plasticity 24 (2008) 1642–1693.
[6] K. Naumenko, H. Altenbach, A. Kutschke, International Journal of Damage Mechanics 20 (2011) 578–597.
[7] F. Längler, K. Naumenko, H. Altenbach, M. Ievdokymov, The Journal of Strain Analysis for Engineering Design 49 (2014) 410–420.
[8] Z.L. Kowalewski, D.R. Hayhurst, B.F. Dyson, The Journal of Strain Analysis for Engineering Design 29 (1994) 309–316.
[9] L. Zhan, J. Lin, T.A. Dean, International Journal of Machine Tools and Manufacture 51 (2011) 1–17.
[10] J. Zhang, Y. Deng, X. Zhang, Materials Science and Engineering: A 563 (2013) 8–15.
[11] H. Altenbach, S. Kozhar, K. Naumenko, International Journal of Damage Mechanics 22 (2013) 683–698.
[12] J. Dünnwald, E. El-Magd, Computational Materials Science 7 (1996) 200–207.
[13] E. El-Magd, A. Kranz, Materialwissenschaft und Werkstofftechnik 31 (2000) 96–101.
[14] N. Anjabin, A. Karimi Taheri, Materials & Design 31 (2010) 433–437.
[15] H. Altenbach, K. Naumenko, Computational Mechanics 19 (1997) 490–495.
[16] H. Altenbach, O. Morachkovsky, K. Naumenko, A. Sychov, Archive of Applied Mechanics 67 (1997) 339–352.
[17] K. Naumenko, H. Altenbach, Modelling of Creep for Structural Analysis, Springer, Berlin, 2007.
[18] J. Betten, Creep Mechanics, Springer, Berlin, 2008.
[19] A. Angella, E. Bassani, E. Gariboldi, D. Ripamonti, in: J. Hirsch, B. Skrotsky, G. Gottstein (Eds.), Aluminium Alloys, vol. 1, Wiley-VCH, 2008, pp. 1067–1092.
[20] K. Naumenko, H. Altenbach, Archive of Applied Mechanics 75 (2005) 808–819.
[21] F.K.G. Odqvist, Mathematical Theory of Creep and Creep Rupture, Oxford University Press, Oxford, 1974.
[22] H.J. Frost, M.F. Ashby, Deformation-Mechanism Maps, Pergamon, Oxford, 1982.
[23] J.W. Hutchinson, Proceedings of the Royal Society of London. A. Mathematical and Physical Sciences 348 (1976) 101–127.
[24] B. Illschner, Hochtemperatur-Plastizität, Springer, Berlin, 1973.
[25] O. Ozhoga-Maslovskajaa, K. Naumenko, H. Altenbach, O. Prygorniev, Computational Materials Science, 2014. In press.
[26] H. Gao, Y. Huang, W.D. Nix, J.W. Hutchinson, Journal of the Mechanics and Physics of Solids 47 (1999) 1239–1263.
[27] S. Forest, Journal of Engineering Mechanics 135 (2009) 117–131.
[28] H. Altenbach, V. Eremeyev, International Journal of Plasticity, 2014.
[29] W. Blum, in: F. Abe, T.-U. Kern, R. Viswanathan (Eds.), Creep-Resistant Steels, Woodhead Publishing, Cambridge, 2008, pp. 365–402.
[30] H.S. Kim, Y. Estrin, Acta Materialia 53 (2005) 765–772.
[31] H. Altenbach, K. Naumenko, P. Zhilin, Continuum Mechanics and Thermodynamics 15 (2003) 539–570.
[32] Y. Estrin, in: A.S. Krausz, K. Krausz (Eds.), Unified Constitutive Laws of Plastic Deformation, Academic Press, San Diego, 1996, pp. 69–104.
[33] M.E. Kassner, M.T. Pérez-Prado, Fundamentals of Creep in Melals and Alloys, Elsevier, Amsterdam, 2004.
[34] B.F. Dyson, M. McLean, in: A. Strang, J. Cawley, G.W. Greenwood (Eds.), Microstructural Stability of Creep Resistant Alloys for High Temperature Plant Applications, Cambridge University Press, Cambridge, 1998, pp. 371–393.
[35] E. Gariboldi, D. Ripamonti, L. Signorelli, G. Vimercati, F. Casaro, Metallurgical Science and Tecnology 25 (2003) 3–11.
[36] H. Altenbach, C. Huang, K. Naumenko, The Journal of Strain Analysis for Engineering Design 37 (2002) 265–275.